https://doi.org/10.5194/wes-2021-34
Preprint. Discussion started: 28 April 2021
© Author(s) 2021. CC BY 4.0 License.

WIND ENERGY SCIENCE DISCUSSIONS

Dynamic inflow model for a Floating Horizontal Axis Wind Turbine in surge motion

Carlos Ferreira[1], Wei Yu[1], Arianna Sala[1], and Axelle Viré[1]
[1]Delft University of Technology, Faculty of Aerospace Engineering, Kluyerweg 1, 2629 HS Delft, the Netherlands
Correspondence: Carlos Ferreira (c.j.simaoferreira@tudelft.nl)

Abstract. Floating Offshore Wind Turbines may experience large surge motions which, when faster than the local wind speed, cause rotor-wake interaction. Previous research hypothesised that this phenomena can result in a turbulent wake state or even a vortex ring state, invalidating the Actuator Disc Momentum Theory and the use of the Blade Element Momentum Theory. We challenge this hypothesis and demonstrate that the Actuator Disc Momentum Theory is valid and accurate in predicting the induction at the actuator in surge, even for large and fast motions. To achieve this, we derive a dynamic inflow model which mimics the vorticity-velocity system and the effect of the motion. The predictions of the model are compared against results from other authors and from a semi-free wake vortex-ring model. The results show that the surge motion and rotor-wake interaction do not cause a turbulent wake state or vortex ring state, and that the application of Actuator Disc Momentum Theory and Blade Element Momentum Theory is valid and accurate, when correctly applied in an inertial reference frame. The results show excellent agreement in all cases. The proposed dynamic inflow model includes an adaptation for highly loaded flow and it is accurate and simple enough to be easily implemented in most Blade Element Momentum models.

1 Introduction

1.1 Motivation for the research

Floating offshore wind turbines (FOWTs) are placed on floating foundations, which leads to larger motions than wind turbines on bottom mounted foundations (de Vaal et al., 2014). This increased freedom of motion can result in several phenomena of unsteady aerodynamics at airfoil, blade, rotor and wake scale, studied by Sebastian and Lackner (2012), Sebastian and Lackner (2013), Sivalingam et al. (2018), Kyle et al. (2020), Wen et al. (2017), Lee and Lee (2019), de Vaal et al. (2014), Mancini et al. (2020), Micallef and Sant (2015), Tran and Kim (2016), Chen et al. (2021), Shen et al. (2018), Lee and Lee (2019), Farrugia et al. (2016), Cormier et al. (2018), Dong et al. (2019), Dong and Viré (2021) and others.

The complexity of the aerodynamics resulted in many interpretations of the phenomena. Several authors proposed that, due to the motion and change in loading, the flow could vary from windmill to propeller state. Also, that if the surge velocity would be large enough, the combination of wind speed and surge velocity would be lower than twice the induction velocity, resulting

https://doi.org/10.5194/wes-2021-34
Preprint. Discussion started: 28 April 2021
© Author(s) 2021. CC BY 4.0 License.

in a turbulent wake state or even a vortex ring state. Many authors stipulated that Actuator Disc Momentum Theory would no longer be valid in these conditions. Since Blade Element Momentum Theory (BEM, see Glauert (1935)) is based on Actuator Disc Momentum Theory, the occurrence of turbulent wake state and vortex ring state would significantly limit the use of BEM for FOWTs. As BEM is the most used tool for the simulation of aerodynamics of horizontal axis wind turbines (Madsen et al., 2020), this could significantly impact our design methods.

However, the prediction of turbulent wake state and vortex ring state for the actuator disc (wind turbine) in periodic surge motion appears to be in most cases the result of an invalid interpretation of the Actuator Disc Theory. As stated by Sørensen and Myken (1992), since the concept of the actuator disc was first formulated by Froude it has been closely related to the one-dimensional momentum theory and much confusion about its applicability in describing complex flow fields still exists. This is particularly true for the case of an actuator in cyclic motion, as is the case of FOWTs.

The name of the theory is in itself misleading, because the Actuator Disc Momentum theory is in fact the theory of the mass and momentum balance of the streamtube that includes the actuator. The actuator disc is a physical model that enables a discontinuity of the pressure field into the governing flow equations as the reaction to an external force field. The added information that the pressure discontinuity occurs at the actuator allows us to estimate the velocity at the actuator by evaluating stagnation pressure along the streamtube. Therefore, Actuator Disc Theory refers to the state of the streamtube defined in an inertial reference frame that contains the actuator which is static in the same inertial reference frame. Propeller state, windmill state, turbulent wake state, vortex ring state and propeller brake state do not refer to the state of the actuator but to the state of the streamtube (Sørensen et al., 1998). In an unsteady flow, an actuator might have an instantaneous loading as a propeller, while the streamtube remains in windmill state. Two examples of such inertial reference frames are the one attached to the steady streamtube which includes the actuator disc associated with a stationary wind turbine (or propeller) in an incoming unperturbed wind speed U_∞ of any value, or the one attached to the steady streamtube that contains an actuator disc in a constant motion (not accelerated) in an incoming unperturbed wind speed U_∞ of any value.

When the actuator is moving in an inertial reference frame with a steady velocity, the streamtube and actuator are in the same inertial reference frame, and the reference unperturbed velocity of the wind used in the actuator disc model $U_{\infty_{ref}}$ is the sum of the velocity of the wind in the inertial reference frame U_∞ with the velocity of the actuator in the inertial reference frame v_{act}, as

$$U_{\infty_{ref}} = U_\infty - v_{act} \tag{1}$$

In this condition, the actuator disc momentum theory applies, and the thrust coefficient C_T is defined as

$$C_T = \frac{T}{\frac{1}{2}\rho U_{\infty_{ref}}^2 A} = 4a\,(1-a) \tag{2}$$

https://doi.org/10.5194/wes-2021-34
Preprint. Discussion started: 28 April 2021
© Author(s) 2021. CC BY 4.0 License.

where T is the thrust applied by the actuator, A is the area of the actuator and a is defined as the induction factor, such that the velocity perceived by the actuator U_{act} (at the location of the actuator) is given by

$$U_{act} = (1-a)\,U_{\infty_{ref}} \tag{3}$$

Strictly speaking, the Actuator Disc Theory cannot be applied to a non-inertial reference frame (e.g. the actuator disc in a periodic surge motion) as this violates the steady assumption. The transition to the accelerated reference frame of the actuator requires the addition of apparent forces in the momentum equation, which are not accounted in the Actuator Disc Momentum theory. Therefore, for FOWTs experiencing accelerated motions, Equation 1 to 3 are invalid for predicting the induction at the oscillating actuator using 1D momentum theory.

Another common misconception is that a perceived negative velocity at the actuator (e.g. the actuator moving downwind faster than the wind during the oscillatory surge motion) represents a vortex ring state. However, the vortex ring state is a property of the streamtube, evaluated in the inertial reference frame of the streamtube. If there is no flow reversal in the streamtube, there is no vortex ring state. For an interpretation of vortex ring state see the works of Sørensen et al. (1998) and Sørensen and Myken (1992). Equally, although the load on the actuator can range from negative (propeller) to highly loaded, that does not mean that the streamtube will vary from propeller state to turbulent wake state. If the oscillation of the loading is very fast, the flow does not have enough time to accelerate and the streamtube will remain in windmill state.

Although the actuator disc model is one-dimensional and assumes steady, incompressible and inviscid flow, when used in engineering applications in unsteady flow, the steady assumption is relaxed and the model can be corrected by dynamic inflow models. If a dynamic inflow model could solve the streamtube induction and the induction at the location of the actuator, BEM could then be used for the simulation of FOWTs. The motivation of this work is to achieve this goal.

1.2 Aim of the research, research questions and hypothesis

The aim of the research is to:

1. Derive and apply a dynamic inflow model as a correction for the effect of surge on the estimation of the induction at the actuator disc.
2. Validate the approach by comparison with the results of higher fidelity models.
3. Demonstrate that, for the cases investigated here (including cases with large surge velocities and loading), turbulent wake state and vortex-ring state do not occur as a consequence of the surge motion, and therefore BEM is still valid.

The main research questions are:

1. Which assumptions of 1D Actuator Disc Momentum Theory are violated in the case of a periodic surge motion and are they critical?

https://doi.org/10.5194/wes-2021-34
Preprint. Discussion started: 28 April 2021
© Author(s) 2021. CC BY 4.0 License.

2. How can the violated assumptions be compensated by a correction model?

3. How can an approach based on a dynamic inflow model be sufficient to extend the actuator disc model to the case of an actuator in surge?

The research aims to test the following hypothesis in connection to the research questions:

1. The surging actuator disc generates an unsteady flow, breaking the steady flow assumption of the actuator disc model. However, the 1D steady actuator disc model might be a suitable basis for modelling taking into account that in most applications: the surge amplitude is small; the amplitude of thrust coefficient is proportional to the frequency of oscillation (in fact, proportional to the maximum surge velocity), leading to small variations of induction even for large amplitudes of the oscillation due to the inertia of the flow.

2. The solution of the actuator disc in a periodic surge motion is best understood in the inertial reference frame when doing a momentum analysis, as it avoids the addition of apparent forces in the momentum equation in an accelerated reference frame.

3. Even for large amplitudes of thrust reaching thrust coefficients $C_T > 1$, the streamtube remains in wind turbine mode. The occurrence of turbulent wake state or vortex ring state is not defined by the fact that the surge velocity is larger than U_∞. The streamtube intersecting the edge of the actuator does not experience breakdown nor flow reversal, except in the case of heavy loading over a long period of time.

4. A lagrangian formulation of the wake generation and the consequent solution of the induction field is invariant with reference frame, be it accelerated or inertial. A dynamic inflow model inspired by lagrangian vorticity distribution should provide a reasonable estimate of the induction at the actuator.

5. The wake solution and the induction solution are the linear superposition of a newly released wake (new wake) and a previously released wake (old wake), in relation to the reduced time scale of the flow.

6. A dynamic inflow model based on a low pass filtering approach (e.g. the Madsen dynamic inflow model) can be modified to account for the dynamics of displacement of the actuator.

7. Because the thrust varies in time, the induction will vary radially, even if the actuator is uniformly loaded.

8. The method can be accurate for a large range of surge motions and thrust variations, beyond the case when thrust is proportional to the maximum surge velocity.

9. The 1D actuator disc model with dynamic inflow model will match solutions of higher fidelity models, such as prescribed and (semi-) free-wake vortex-ring models.

The hypothesis described above make reference to amplitude and frequency of the surge motion and loading experienced by FOWTs. In Section 1.3 we define the surge motion and thrust functions. Section 1.4 presents a summary of study cases found in literature, organised in distributions of the range of parameters that define the surge motion and thrust function.

https://doi.org/10.5194/wes-2021-34
Preprint. Discussion started: 28 April 2021
© Author(s) 2021. CC BY 4.0 License.

1.3 Description of the motion of the actuator and loading on the actuator

The simulations and analysis in this work use the following assumptions. The actuator surface is a circle of diameter D (radius $R = D/2$), and is always normal to the unperturbed free-stream U_∞. The latter is uniform, steady, and aligned with the x-direction. The actuator moves in the x-direction according to Equation 4, where x_{act} is the location of the actuator in the x-axis, $A_{x_{act}}$ is the amplitude of the motion and Ω is the frequency of the motion, defined in relation to a reduced frequency k as stated in Equation 5. The loading over the actuator is uniform and normal to the surface, and the thrust coefficient C_T is defined by Equation 6 taking U_∞ as reference for the dynamic pressure, where C_{T_0} is the average thrust coefficient, ΔC_T is the amplitude of the variation of C_T, ϕ is an additional phase difference between motion and loading, and t represents time.

$$x_{act} = A_{x_{act}} \sin\left(\frac{kU_\infty}{D} t\right) \tag{4}$$

$$k = \frac{\Omega D}{U_\infty} \tag{5}$$

$$C_T = \frac{T}{\frac{1}{2}\rho U_\infty^2 A} = C_{T_0} - \Delta C_T \cos\left(\frac{kU_\infty}{D} t + \phi\right) \tag{6}$$

1.4 Survey of study cases in previous experimental and numerical research

Figure 1 presents a survey of the experimental and numerical study cases in the work of de Vaal et al. (2014), Kyle et al. (2020), Mancini et al. (2020), Micallef and Sant (2015), Tran and Kim (2016), Chen et al. (2021), Sivalingam et al. (2018), Shen et al. (2018), Lee and Lee (2019), Farrugia et al. (2016), Wen et al. (2017), Cormier et al. (2018) and Dong et al. (2019). The results are organised in $\frac{A_{x_{act}}}{D}$ vs. k with isocurves of v_{max} in Figure 1a, ΔC_T vs $v_{max} = \frac{\Omega A_{x_{act}}}{U_\infty}$ in Figure 1b and ΔC_T vs. C_{T_0} in Figure 1c . Orange symbols represent Eulerian Navier-Stokes simulations (commonly referred to as CFD), green symbols represent Lagrangian vortex models, and blue symbols represent experiments (some also including simulations). Figure 1b is inspired by the work of Mancini et al. (2020). The survey shows that amplitudes of the motion are below $0.13D$ and reduced frequency $k < 15$. More importantly, the maximum surge velocity is $v_{max} < 1.15$. The relation of ΔC_T to C_{T_0} shows that only in three cases the thrust reaches negative values. The almost linear relation of ΔC_T to v_{max} confirms the earlier observations by Mancini et al. (2020). An hypothesis is that the linear relation is explainable by the linear effect between the surge velocity and the circulation on the blades, due to the change of the non-entry boundary condition on the blade surface.

In this work we will evaluate the proposed Actuator Disc Momentum theory with dynamic inflow correction in a motion and load space wider than (and encompassing) the one in Figure 1. The next section presents the Methods used in the research. It is followed by the Results and Discussion and finally the Conclusions.

https://doi.org/10.5194/wes-2021-34
Preprint. Discussion started: 28 April 2021
© Author(s) 2021. CC BY 4.0 License.

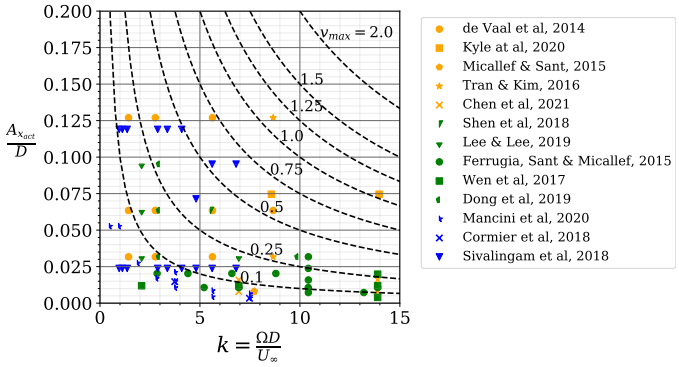

(a) $\frac{A_{x_{act}}}{D}$ vs. k with isocurves of $v_{max} = \frac{\Omega A_{x_{act}}}{U_\infty}$.

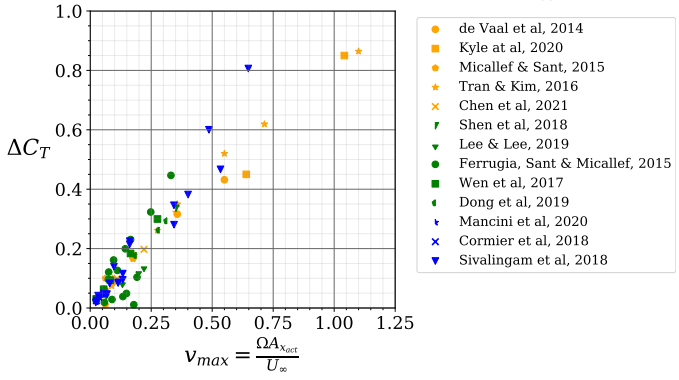

(b) ΔC_T vs. $v_{max} = \frac{\Omega A_{x_{act}}}{U_\infty}$.

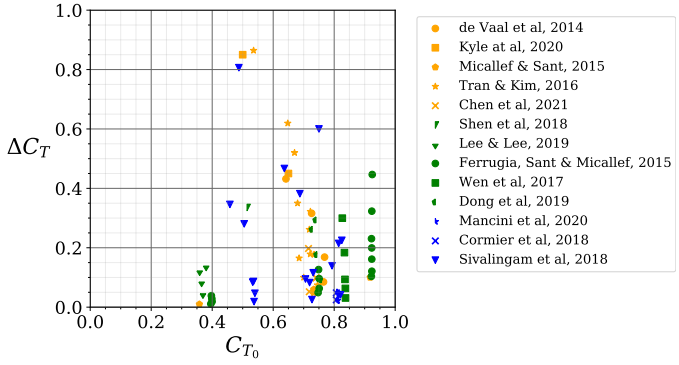

(c) ΔC_T vs. C_{T_0}.

Figure 1. Survey of the experimental and numerical study cases in the work of de Vaal et al. (2014), Kyle et al. (2020), Mancini et al. (2020), Micallef and Sant (2015), Tran and Kim (2016), Chen et al. (2021), Sivalingam et al. (2018), Shen et al. (2018), Lee and Lee (2019), Farrugia et al. (2016), Wen et al. (2017), Cormier et al. (2018) and Dong et al. (2019). The results are organised in $\frac{A_{x_{act}}}{D}$ vs. k with isocurves of v_{max} (sub-figure *a)*), ΔC_T vs $v_{max} = \frac{\Omega A_{x_{act}}}{U_\infty}$ (sub-figure *b)* and ΔC_T vs. C_{T_0} (sub-figure *c)*). Orange symbols represent Eulerian Navier-Stokes simulations (commonly referred to as CFD), green symbols represent Lagrangian vortex models, and blue symbols represent experiments (some also including simulations).

https://doi.org/10.5194/wes-2021-34
Preprint. Discussion started: 28 April 2021
© Author(s) 2021. CC BY 4.0 License.

2 Methods and approach

The results presented and discussed in the Section Results and Discussion have three sources: the Navier-Stokes simulations of an actuator disc in surge by de Vaal et al. (2014); simulations by a semi-free wake vortex-ring model of an actuator disc in surge motion developed in this work; and a 1D Actuator Disc Momentum model corrected for the unsteady surge motion and loading by using a dynamic inflow model derived in this work. The cases are defined by the surge motion and unsteady load on the actuator. The results and discussion compare the estimate of induction at the actuator disc. The higher fidelity results are used as benchmark for the results of the proposed dynamic inflow model.

2.1 Semi-free wake vortex ring model

The semi-free wake vortex ring model is a conventional model inspired by the approaches in the works of Yu et al. (2016), Yu (2018), van Kuik (2018) and van Kuik (2020). The "semi-free wake" description is due to the fact that the wake expands and convects with self induction up to five diameters downstream of the actuator. After that location, the expansion is frozen and the wake convects with a velocity based on U_∞ and the velocity at the center of the wake.

2.2 Algorithm for the dynamic inflow model

The work of Madsen et al. (2020) presents an updated version of the Madsen (Larsen-Madsen) dynamic inflow model, following up on the work by Pirrung and Madsen (2018). The Madsen dynamic inflow model is conceptualized as a curve fit of the solution of an unsteady actuator disc in a step function that uses two time scales to better approximate the radial dependency of the unsteady induction, implicitly as a near wake and far wake time scales. This is also the interpretation proposed in the work of De Tavernier and Ferreira (2020) when reviewing the implementation for Vertical Axis Wind Turbines (see also Larsen and Madsen (2013)), discussing the time scales as near wake and far wake. The model presented by Pirrung and Madsen (2018) predicts several corrections for loading and radial effects and is calibrated against higher fidelity simulations.

In this work we take inspiration of the two time scales approach to separate the induction at streamtube scale from the induction at the actuator. We therefore define two reference values of induction, namely the streamtube induction velocity u_{str} and the induction velocity at the location of the actuator u_{act}. We use these velocities to determine the convection of the vorticity system in the streamtube and in relation to the actuator.

The first step of the algorithm is to define an unperturbed reference velocity of the inertial reference frame that contains the streamtube and the actuator. In the case of the actuator in an oscillating surge, the reference velocity can be defined as in Equation 7

$$U_{\infty_{ref}} = U_\infty \tag{7}$$

https://doi.org/10.5194/wes-2021-34
Preprint. Discussion started: 28 April 2021
© Author(s) 2021. CC BY 4.0 License.

The second step of the algorithm is to define a streamtube wake-convection reference velocity at the actuator, as defined in Equation 8, where we average the two induction velocities.

$$U_{str} = U_{\infty_{ref}} - \frac{u_{str} + u_{act}}{2} \tag{8}$$

We can calculate an equivalent quasi-steady solution of the induction velocity (Equation 9) to be later used as a forcing function in the filter functions. It is important to note that this forcing function differs from the one commonly used in dynamic inflow models (usually the steady induction for a given thrust coefficient as defined in Equation 2).

$$u_{qs} = \frac{C_T U_\infty^2}{4} \frac{1}{U_{str}} \tag{9}$$

We can choose to apply a form of Glauert's correction for the case of heavily loaded streamtubes and $C_T > 0$, inspired in the formulation presented by Burton et al. (2011). The heavily loaded streamtube criterion is defined as

$$U_{str} > U_{\infty_{ref}} \left(1 - \frac{\sqrt{C_{T_1}}}{2}\right) \tag{10}$$

with $C_{T_1} = 1.816$.

If the criterion in Equation 10 applies, the value of u_{qs} can be determined by Equation 11, curve fitted from Glauert's correction as described by Burton et al. (2011).

$$u_{qs} = -1.883 - 1.540\sqrt{\frac{C_T U_\infty^2}{4} \frac{1}{U_{str}}} + 4.086\sqrt[4]{\frac{C_T U_\infty^2}{4} \frac{1}{U_{str}}} \tag{11}$$

We must now define length scales for actuator/near wake scale L_{act} and streamtube/far wake scale L_{str} in Equations 12 and 13. The choice of one and five diameters are suitable for near and far wake scales. The length scales are defined as half of the near and far wake scales for application in the exponential functions of the filter functions.

$$L_{act} = \frac{1}{2} 1D \tag{12}$$

$$L_{str} = \frac{1}{2} 5D \tag{13}$$

We now define time scales of convection of the wake for actuator/near wake scale and streamtube/far wake scale. For the streamtube scale we define one time scale τ_{str} given by Equation 14, used for the convection of the old vorticity system and the convection of the generation of the new vorticity system.

$$\tau_{str} = \frac{L_{str}}{U_{\infty_{ref}} - \frac{u_{str}}{2}} \tag{14}$$

https://doi.org/10.5194/wes-2021-34
Preprint. Discussion started: 28 April 2021
© Author(s) 2021. CC BY 4.0 License.

For the actuator/near wake scale we need to define two time scales: one for the convection of the old vorticity system (Equation 15) and another for the convection of the generation of the new vorticity system (Equation 16). The velocity of the actuator is defined as the time derivative of position of the actuator $v_{act} = \frac{\mathrm{d}x_{act}}{\mathrm{d}t}$

$$\tau_{act_1} = \frac{L_{act}}{U_\infty - \frac{u_{act}}{2} - v_{act}} \tag{15}$$

$$\tau_{act_2} = \frac{L_{act}}{U_{\infty_{ref}} - \frac{u_{act}}{2}} \tag{16}$$

We can now calculate the new solutions of the streamtube induction velocity u_{str} and the induction velocity at the location of the actuator u_{act} by a low pass filter.

$$u_{act_{(t+\Delta t)}} = u_{act_{(t)}} e^{-\frac{\Delta t}{\tau_{act_1}}} + u_{qs}\left(1 - e^{-\frac{\Delta t}{\tau_{act_2}}}\right) \tag{17}$$

$$u_{str_{(t+\Delta t)}} = u_{str_{(t)}} e^{-\frac{\Delta t}{\tau_{str}}} + u_{qs}\left(1 - e^{-\frac{\Delta t}{\tau_{str}}}\right) \tag{18}$$

When $U_{\infty_{ref}} = U_\infty$, Equation 17 can also be written as Equation 19.

$$u_{act_{(t+\Delta t)}} = u_{act_{(t)}} e^{-\frac{\Delta t}{\tau_{act_2}}} e^{\Delta t \frac{v_{act}}{L_{act}}} + u_{qs}\left(1 - e^{-\frac{\Delta t}{\tau_{act_2}}}\right) \tag{19}$$

Equation 19 shows the effect of the actuator motion. As the actuator moves away form the previously shed wake, the effective induction decreases. As the actuator moves into the wake, the effective induction increases.

The algorithm can be generalised to the case of other actuator motions, e.g. an actuator travelling in forward motion with periodic oscillations. In this case, the most suitable inertial reference frame needs to be updated and so does $U_{\infty_{ref}}$. A third filtering can be applied in the form of Equation 20

$$U_{\infty_{ref(t+\Delta t)}} = U_{\infty_{ref(t)}} e^{-\Delta t \frac{U_{\infty_{ref(t)}}}{L_{str}}} + (U_\infty - v_{act})\left(1 - e^{-\Delta t \frac{U_{\infty_{ref(t)}}}{L_{str}}}\right) \tag{20}$$

An example of the implementation of the algorithm in Python is shown in *Appendix A: Implementation of the algorithm in Python*.

In the Results section, the induction at the actuator is represented by its non-dimensioned form a, defined by Equation 21.

$$a = \frac{u_{act}}{U_\infty} \tag{21}$$

https://doi.org/10.5194/wes-2021-34
Preprint. Discussion started: 28 April 2021
© Author(s) 2021. CC BY 4.0 License.

3 Results and Discussion

3.1 Comparison of results of the dynamic inflow model with those of de Vaal et al. (2014).

This section compares the results of the dynamic inflow model with the results of the semi-free wake model and the results published in de Vaal et al. (2014), page 117, for a moving actuator disc modelled in the commercial software FLUENT using a finite volume discretization of the incompressible Navier-Stokes equations. The study case is an actuator disc in a sinusoidal surge motion and varying thrust. The four sub-cases have the same motion amplitude but four different motion frequencies. Figure 2 describes the four sub-cases and presents the thrust curve and the resulting values of induction coefficient over the rotation. The location of the actuator x_{act} is also plotted.

There are two important differences between the simulations in this work and the ones in (de Vaal et al., 2014). The simulations with the dynamic inflow model and with the semi-free wake model use an unsteady uniform loading over the actuator, and the inductions plotted in Figure 2 correspond to the induction at the actuator at different radial positions. de Vaal et al. (2014) applied a rotor model (NREL 5MW) in their model, leading to an non-uniform loading. Additionally, the induction plotted in Figure 2 is the area weighted induction at the blade, including Prandtl's tip correction for finite blade effects. The non-uniform loading considered by de Vaal et al. (2014) and the inclusion of Prandtl's tip correction leads to a higher value of induction in relation to the average induction over the annulus. By studying the solution for the steady load case presented in the work of de Vaal et al. (2014) (Figure 4, page 112), it is possible to estimate the average induction using their approach to be between $a = 0.274$ and $a = 0.285$ (depending on tip correction model), while an actuator disc with uniform load and the same thrust coefficient ($C_T = 0.76$) will result in an induction of $a = 0.256$. This results in a $\Delta a \approx 0.023$ between the two methodologies.

To support the interpretation of the results in Figure 2, Table 1 presents for each sub-case (labelled by the reduced frequency k) the average thrust coefficient $\overline{C_T}$, the amplitude of the variation of thrust coefficient ΔC_T, the time average of the area-weighted and Prandtl-tip-corrected average induction $\overline{\bar{a}_{deVaal}}$, the time average of the area-weighted average induction obtained with the semi-free wake vortex ring model $\overline{\bar{a}_{sfwm}}$, the time average of the induction at the center of the actuator predicted by the dynamic inflow model $\bar{a}_{dynamic\ inflow}$, the time average of the induction calculated using steady Actuator Disc Theory $\overline{a_{(C_T)}}_{steady}$ and the steady induction of the time average of thrust coefficient $a_{(\overline{C_T})steady}$ (the last two predicted using steady 1D actuator disc theory).

The results in Figure 2 and Table 1 show that:

1. Comparing the results of de Vaal et al. (2014) and the vortex ring model, despite the difference of what is modelled (non-uniform loading vs. uniform loading) and the difference of the nature of the two values of induction (impact of Prandtl's tip correction), it results that $\overline{\bar{a}_{deVaal}} - \overline{\bar{a}_{sfwm}} < 0.02$.

2. Although the dynamic inflow model is one-dimensional, the difference to the semi-free wake vortex ring model prediction is, in all cases, less than $\Delta a < 0.01$ for the region $r/R \leqslant 0.8$.

https://doi.org/10.5194/wes-2021-34
Preprint. Discussion started: 28 April 2021
© Author(s) 2021. CC BY 4.0 License.

Table 1. Table of averages of the results of Figure 2.

k	$\overline{C_T}$	ΔC_T	$\overline{\overline{a}_{deVaal}}$	$\overline{\overline{a}_{sfwm}}$	$\bar{a}_{dynamic\ inflow}$	$\overline{a_{(C_T)}}_{steady}$	$a_{(\overline{C_T})steady}$
1.43	.77	.09	.286	.268	.262	.264	.261
2.77	.77	.17	.282	.267	.261	.267	.259
5.62	.75	.31	.272	.258	.255	.272	.25
8.66	.69	.43	.258	.239	.236	.254	.222

3. With increasing reduced frequency, there is an increased phase shift between the curve of the motion/thrust and the resulting induction. The dynamic inflow model is able to capture the phase shift, matching what is observed in the results of de Vaal et al. (2014) and of the vortex ring model.

4. The results confirm that with increasing reduced frequency the average induction will differ from $\overline{a_{(C_T)}}_{steady}$ towards $a_{(\overline{C_T})steady}$ despite the higher amplitude ΔC_T, a consequence of the inertia of the streamtube.

The results of the semi-free wake vortex-ring model show a larger oscillation of induction closer to the actuator edge. This is not a finite-blade tip effect, nor the radial variation of induction previously found in a steady actuator disc with uniform loading (van Kuik, 2018). It is actually an effect of blade (actuator) vortex interaction due to the motion of the actuator and unsteady loading.

The results listed above allow us to conclude that for this case study: 1) the semi-free wake vortex ring model provides results in excellent agreement with those of the higher fidelity model used by de Vaal et al. (2014); 2) the predictions of the dynamic inflow model are in excellent agreement with the results of the semi-free wake vortex ring model; 3) accounting for the Δa due to the differences between non-uniform loading vs. uniform loading, the predictions of the dynamic inflow model are in excellent agreement with the results by de Vaal et al. (2014).

In the next section we will compare the predictions of the dynamic inflow model with the results of the semi-free wake vortex ring model for a more diverse and more challenging set of cases.

3.2 Comparison of results of the dynamic inflow model with those of the semi-free wake vortex ring model

In this section we present and discuss the comparison of the results of induction by the semi-free wake vortex ring model and the proposed dynamic inflow model at the center of the actuator $r/R = 0$ for a sinusoidal surge motion with $x_{act} = A_{x_{act}} \sin(kU_\infty/Dt)$ (also plotted) and with $C_T = C_{T_0} - \Delta C_T \cos(kU_\infty/Dt)$, where the loading is uniformly distributed over the actuators.

Figure 3 presents the cases for $x_{act} = 0.1D \sin(kU_\infty/Dt)$ and $C_T = 0.5 - 0.5\cos(kU_\infty/Dt)$ for six values of reduced frequency $k = [1.0, 3.0, 5.0, 10.0, 15.0, 20.0]$. The results show an excellent agreement between the semi-free wake vortex ring model and the proposed dynamic inflow model. The agreement improves with increasing reduced frequency. The model is also able to capture the progressive phase shift of the induction with increased reduced frequency, as the effect of the motion starts to dominate over the effect of varying thrust. Despite the large amplitude of loading and motion, the highest difference

https://doi.org/10.5194/wes-2021-34
Preprint. Discussion started: 28 April 2021
© Author(s) 2021. CC BY 4.0 License.

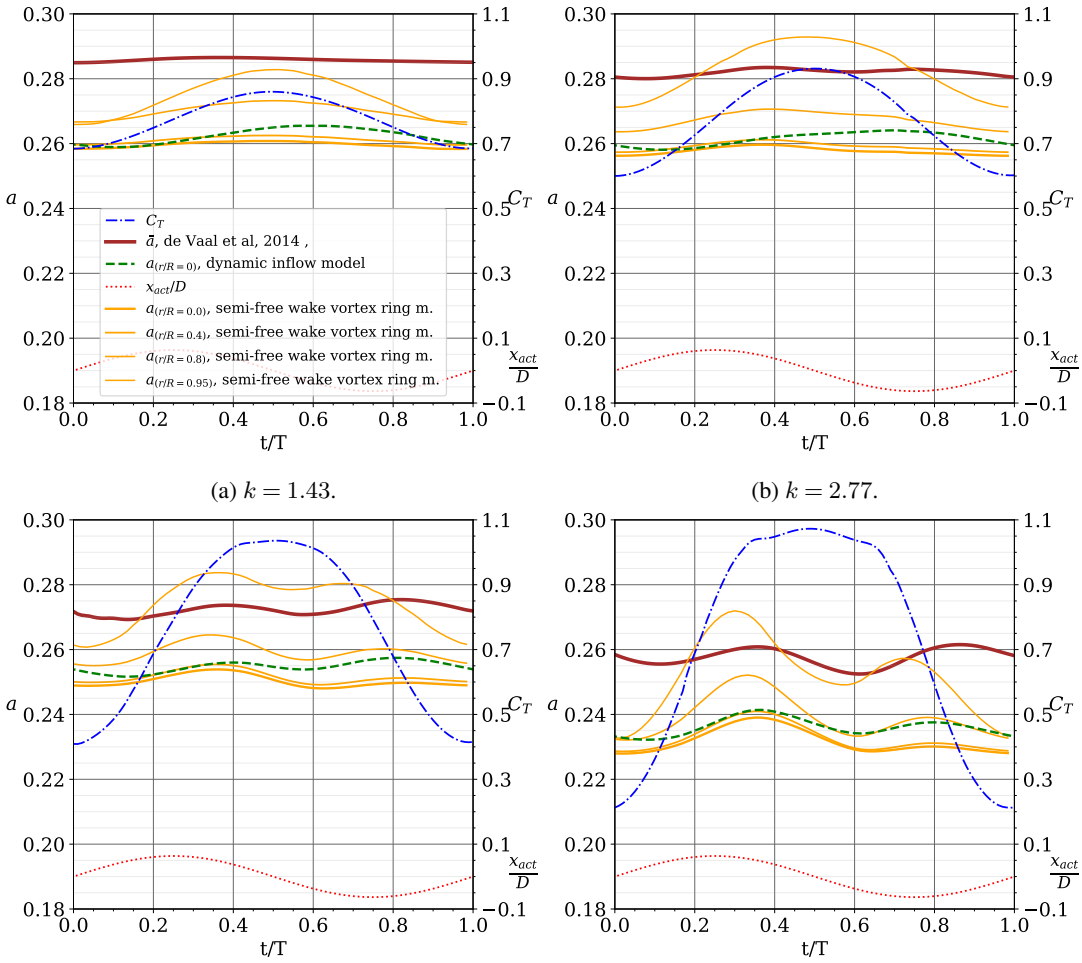

(a) $k = 1.43$.

(b) $k = 2.77$.

(c) $k = 5.63$.

(d) $k = 8.66$.

Figure 2. Comparison of the results of induction by de Vaal et al. (2014) ($\bar{a}$ average induction factor over the actuator), the semi-free wake vortex ring model (a at different radial positions r/R) and the new proposed dynamic inflow model (a at center of the actuator $r/R = 0$). The four case studies are defined by a surge motion of the actuator a sinusoidal motion with $x_{act} = A_{x_{act}} \sin(kU_\infty/Dt)$ with $A_{x_{act}} = 0.063D$, and $k = 1.43$, 2.77, 5.63 and 8.66. The resulting thrust coefficient C_T is also plotted. The results are plotted over one period, along the non-dimensioned time t/T.

https://doi.org/10.5194/wes-2021-34
Preprint. Discussion started: 28 April 2021
© Author(s) 2021. CC BY 4.0 License.

occurs in the case of lowest frequency, with the difference at some points of the cycle being $\Delta a = 0.02$. In this low frequency, the streamtube is significantly accelerated due to the slowly changing load, and the dynamic inflow model must capture this acceleration.

Figure 4 allows us to distinguish the effect of motion from the effect of varying thrust. Figures 4a and 4b allow to compare the effect of increasing the reduced frequency of the motion while the thrust remains constant. Due to motion, the induction is higher when the actuator is in the downwind region (the actuator moves faster than the wake and immerses in its own wake), and lowers as the actuator moves upwind (lower density of vorticity in the near wake). The increasing frequency of motion increases the amplitude of the induction and shifts its phase. Although it shifts towards the phase of the position of the motion, it is actually shifting towards a $\pi/2$ shift in relation to the velocity of the motion. Figures 4c and 4d show the cases of a static actuator where the load is phase shifted by π between the two figures. The inductions are naturally also phase shifted by π. Although trivial, these two cases are important to understand Figures 4e and 4f. Figure 4e corresponds to the typical case experienced by a surging wind turbine, where the loading is highest when the actuator moves upwind and lowest when the actuator moves downwind. The effects of motion on the near wake density and the effects of thrust are out of phase and mostly cancel each other. Figure 4f shows a case that is mostly infeasible in a floating wind turbine (and probably undesirable as it could be unstable), where the thrust and motion are in phase and accumulate. This theoretical case allows us to push the dynamic flow model to one of the more challenging cases as it results in a larger amplitude of induction. However, even in this case, the dynamic inflow model is in good agreement with the results of the semi free wake model.

Figure 5 shows the comparison of the two models for six cases where the amplitude of thrust is proportional to the maximum surge velocity $\Delta C_T = \frac{kA_{x_{act}}}{D}$. The values of amplitude of the motion is the same for all cases $A_{x_{act}} = 0.1D$. The six value of reduced frequency are $k = [1.0, 3.0, 5.0, 10.0, 15.0, 20.0]$ implying $\Delta C_T = [0.1, 0.3, 0.5, 1.0, 1.5, 2.0]$, while the average thrust coefficient is $C_{T_0} = 0.8$. The results show that the increased speed of motion mostly cancels the effect of the varying thrust, and the induction remains almost constant. The two models are in excellent agreement in the prediction of the induction (the difference is below 0.02 in all cases). The increased frequency leads to higher changes of loading, but the variation is so fast that the streamtube does not change the velocity significantly.

4 Conclusions

In this work we proposed the test and verification of several hypotheses (described in the introduction) that would allow us to derive and demonstrate that actuator disc momentum theory extended with a dynamic inflow model can predict the induction on an actuator in surge motion.

The results presented and discussed demonstrated the validity of the hypotheses and the accuracy of the model against the results by de Vaal et al. (2014) and higher fidelity simulations with a semi-free wake model using vortex rings. The accuracy of the model was demonstrated for a large range of combinations of loading and motions, even beyond what would usually be expected in a floating wind turbine. In some cases, the travelling velocity of the actuator was twenty times that of the unperturbed wind speed and the amplitude of thrust variation was more that twice the average loading.

https://doi.org/10.5194/wes-2021-34
Preprint. Discussion started: 28 April 2021
© Author(s) 2021. CC BY 4.0 License.

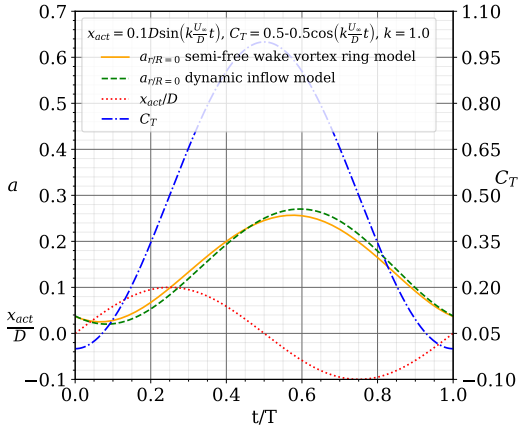

(a) $A_{x_{act}} = .1D$, $k = 1$, $C_{T_0} = .5$, $\Delta C_T = .5$, $v_{max} = 0.1$.

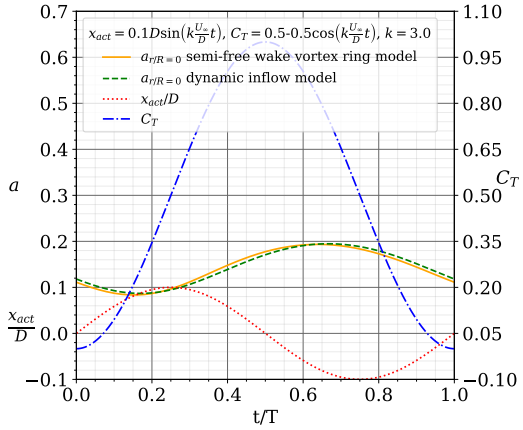

(b) $A_{x_{act}} = .1D$, $k = 3$, $C_{T_0} = .5$, $\Delta C_T = .5$, $v_{max} = 0.3$.

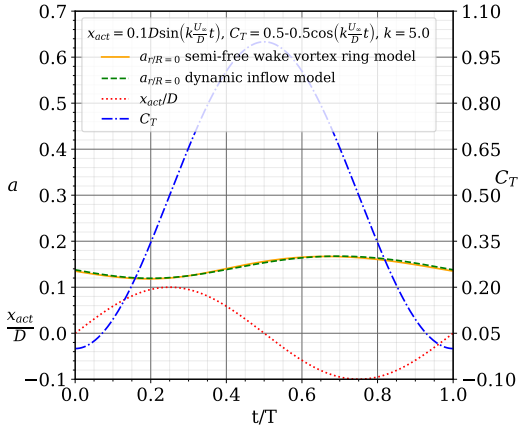

(c) $A_{x_{act}} = .1D$, $k = 5$, $C_{T_0} = .5$, $\Delta C_T = .5$, $v_{max} = 0.5$.

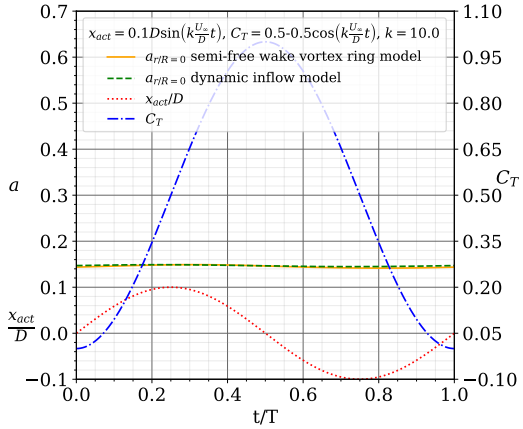

(d) $A_{x_{act}} = .1D$, $k = 10$, $C_{T_0} = .5$, $\Delta C_T = .5$, $v_{max} = 1.0$.

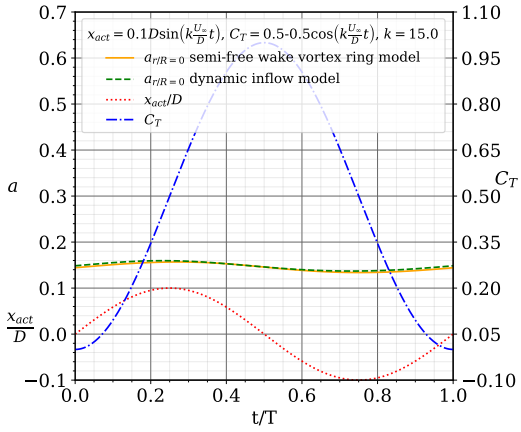

(e) $A_{x_{act}} = .1D$, $k = 15$, $C_{T_0} = .5$, $\Delta C_T = .5$, $v_{max} = 1.5$.

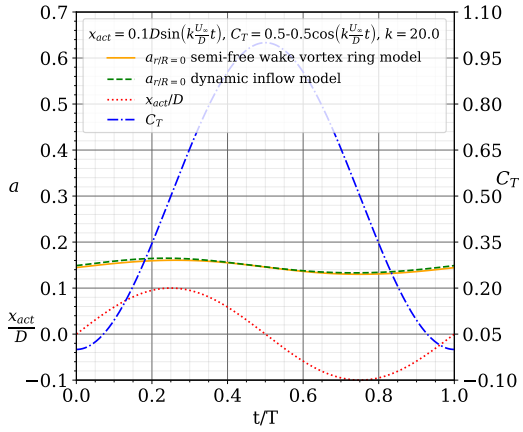

(f) $A_{x_{act}} = .1D$, $k = 20$, $C_{T_0} = .5$, $\Delta C_T = .5$, $v_{max} = 2.0$.

Figure 3. Comparison of the results of induction by the semi-free wake vortex ring model and the proposed dynamic inflow model at center of the actuator $r/R = 0$ for a sinusoidal surge motion with $x_{act} = A_{x_{act}} \sin(kU_\infty/Dt)$ (also plotted) and with $C_T = C_{T_0} - \Delta C_T \cos(kU_\infty/Dt)$ (also plotted). The results are plotted over one period, along the non-dimensioned time t/T. Cases with different reduced frequency.

https://doi.org/10.5194/wes-2021-34
Preprint. Discussion started: 28 April 2021
© Author(s) 2021. CC BY 4.0 License.

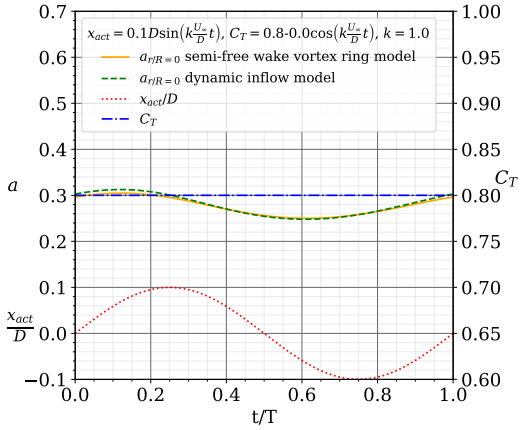

(a) $A_{x_{act}} = .1D$, $k = 1$, $C_{T_0} = .8$, $\Delta C_T = .0$, $v_{max} = 0.1$.

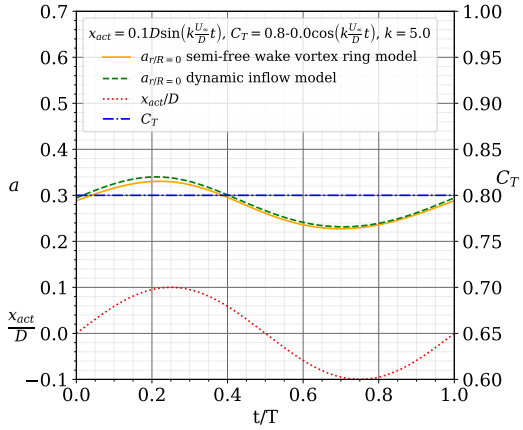

(b) $A_{x_{act}} = .1D$, $k = 5$, $C_{T_0} = .8$, $\Delta C_T = .0$, $v_{max} = 0.5$.

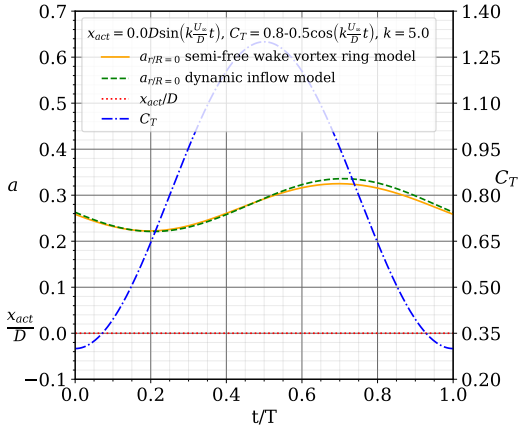

(c) $A_{x_{act}} = 0.0D$, $k = 5$, $C_{T_0} = .8$, $\Delta C_T = .5$, $v_{max} = 0.0$.

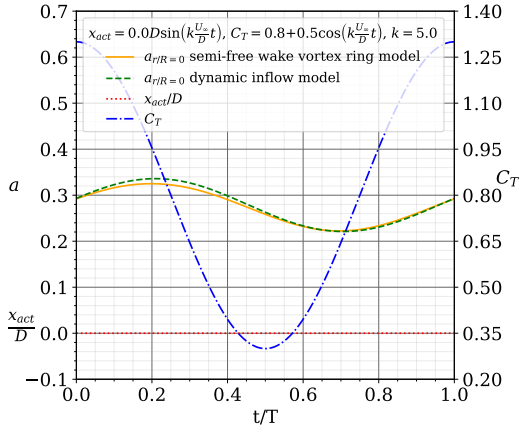

(d) $A_{x_{act}} = 0.0D$, $k = 5$, $C_{T_0} = .8$, $\Delta C_T = -.5$, $v_{max} = 0.0$.

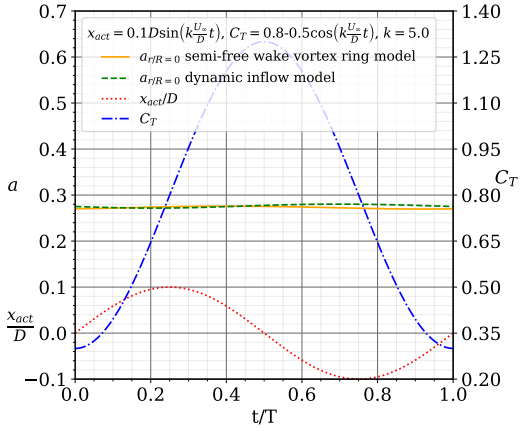

(e) $A_{x_{act}} = .1D$, $k = 5$, $C_{T_0} = .8$, $\Delta C_T = .5$, $v_{max} = 0.5$.

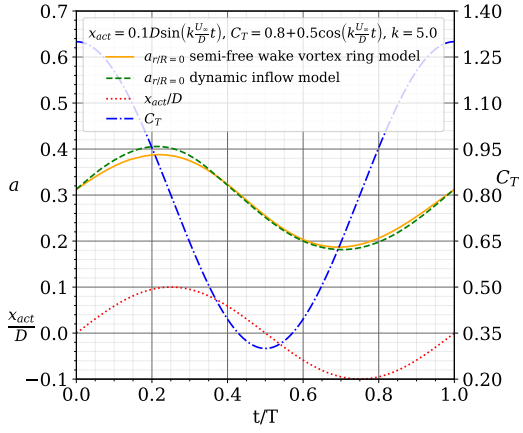

(f) $A_{x_{act}} = .1D$, $k = 5$, $C_{T_0} = .8$, $\Delta C_T = -.5$, $v_{max} = 0.5$.

Figure 4. Comparison of the results of induction by the semi-free wake vortex ring model and the proposed dynamic inflow model at center of the actuator $r/R = 0$ for a sinusoidal surge motion with $x_{act} = A_{x_{act}} \sin(kU_\infty/Dt)$ (also plotted) and with $C_T = C_{T_0} - \Delta C_T \cos(kU_\infty/Dt)$ (also plotted). The results are plotted over one period, along the non-dimensioned time t/T. The results detail the separate effects of motion and load.

https://doi.org/10.5194/wes-2021-34
Preprint. Discussion started: 28 April 2021
© Author(s) 2021. CC BY 4.0 License.

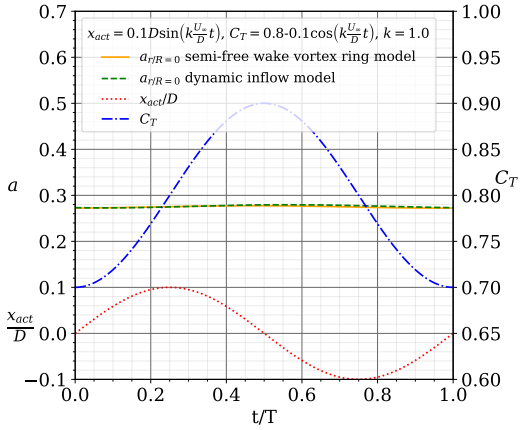

(a) $A_{x_{act}} = .1D$, $k = 1$, $C_{T_0} = .8$, $\Delta C_T = \frac{kA_{x_{act}}}{D}$, $v_{max} = 0.1$.

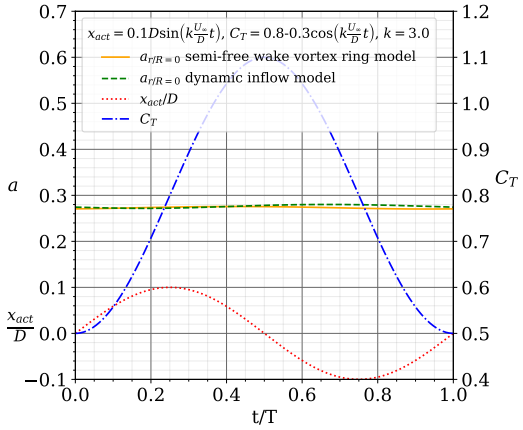

(b) $A_{x_{act}} = .1D$, $k = 3$, $C_{T_0} = .8$, $\Delta C_T = \frac{kA_{x_{act}}}{D}$, $v_{max} = 0.3$.

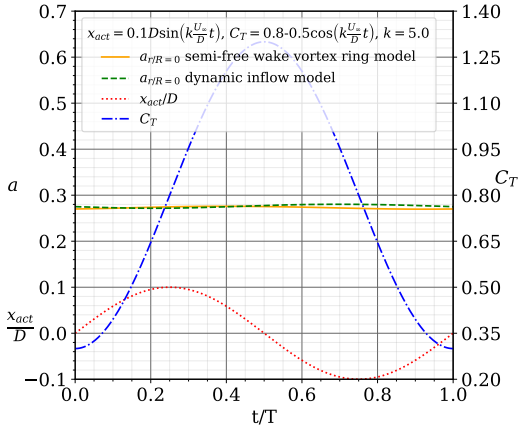

(c) $A_{x_{act}} = .1D$, $k = 5$, $C_{T_0} = .8$, $\Delta C_T = \frac{kA_{x_{act}}}{D}$, $v_{max} = 0.5$.

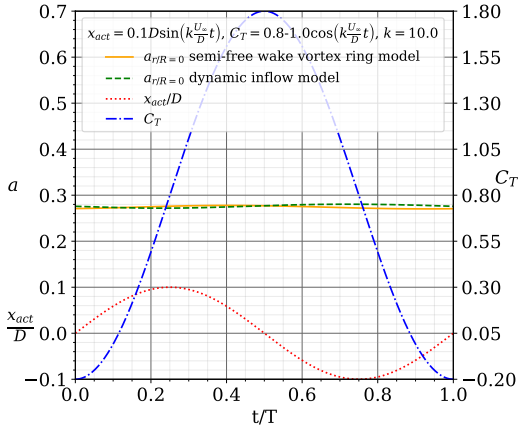

(d) $A_{x_{act}} = .1D$, $k = 10$, $C_{T_0} = .8$, $\Delta C_T = \frac{kA_{x_{act}}}{D}$, $v_{max} = 1.0$.

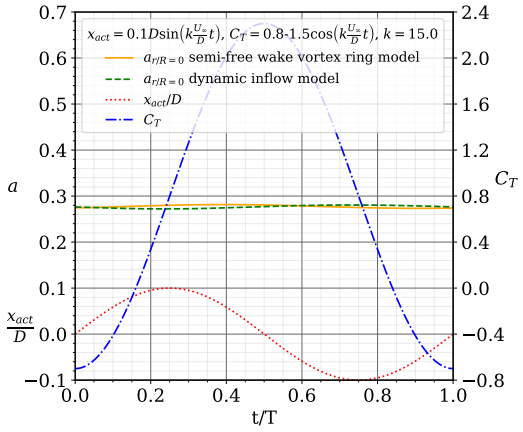

(e) $A_{x_{act}} = .1D$, $k = 15$, $C_{T_0} = .8$, $\Delta C_T = \frac{kA_{x_{act}}}{D}$, $v_{max} = 1.5$.

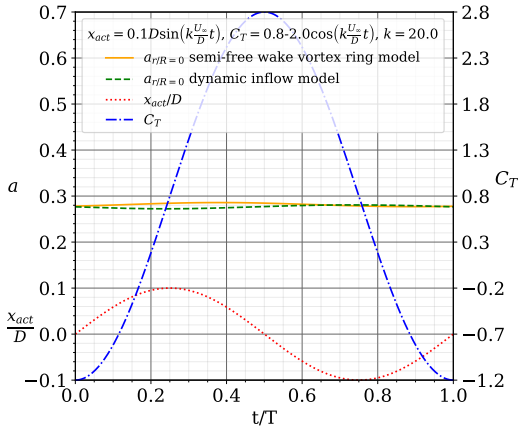

(f) $A_{x_{act}} = .1D$, $k = 20$, $C_{T_0} = .8$, $\Delta C_T = \frac{kA_{x_{act}}}{D}$, $v_{max} = 2.0$.

Figure 5. Comparison of the results of induction by the semi-free wake vortex ring model and the proposed dynamic inflow model at center of the actuator $r/R = 0$ for a sinusoidal surge motion with $x_{act} = A_{x_{act}} \sin(kU_\infty/Dt)$ (also plotted) and with $C_T = C_{T_0} - \Delta C_T \cos(kU_\infty/Dt)$ (also plotted). The results are plotted over one period, along the non-dimensioned time t/T. These cases are defined by $\Delta C_T = \frac{kA_{x_{act}}}{D}$.

https://doi.org/10.5194/wes-2021-34
Preprint. Discussion started: 28 April 2021
© Author(s) 2021. CC BY 4.0 License.

The results also allowed us to confirm that although the increased frequency of motion can lead to higher amplitude of loading and velocity, the inertia of the streamtube results in an almost constant induction. The effect of motion tends to counter the variation of thrust (assuming a ΔC_T proportional to the surge velocity), and the induction at the actuator has a smaller variation with increased frequency.

As hypothesized, there is no occurrence of vortex ring state or even turbulent wake condition. Although this had been raised by previous works, it was actually the result of an incorrect application of actuator disc momentum theory to the accelerated reference frame of the actuator (inspired by the conventional application when the actuator is an inertial reference frame e.g. a flying propeller).

The proposed dynamic inflow model is inspired by the work of Madsen, and in its current formulation, is simpler than the formulation presented by Madsen et al. (2020). The simple algorithm can easily be implemented in BEM models. The proposed dynamic inflow model showed a very good prediction up to $r/R = 0.8$. However, it can be further developed to account for the outer 20% of the radius, including blade vortex interaction. The current implementation already addresses the case of heavier loaded streamtubes; this region remains challenging, even for static actuators.

For future work, the simplicity of the model and its analytical formulation makes it suitable for optimisation and control of FOWTs. The prediction of the induction at the tip region still needs to be improved.

Appendix: Appendix A: Implementation of the algorithm in Python.

```
import numpy as np


def dynamic_inflow_model_moving_actuator(CT, Uinf,Uref,R,dt,u_act,u_str,
                                         v_actuator=0,glauert=False, dynamic=False):
    # calculates the induction velocity at the center of
    # an actuator disc in surge motion
    # developed by:     Carlos Ferreira,
    #                         Delft University of Technology, October 7th 2020
    # inputs:
    #         CT - thrust coefficient of the actuator
    #         Uinf - unperturbed wind speed
    #         Uref - reference unperturbed wind speed in the inertial reference
    #                that contains the streamtube
    #         R -  radius of the actuator
```

https://doi.org/10.5194/wes-2021-34
Preprint. Discussion started: 28 April 2021
© Author(s) 2021. CC BY 4.0 License.

```
#           dt - delta time
#           u_str - streamtube induction velocity (changed in function)
#           u_act - induction velocity at actuator (changed in function)
#           v_actuator - velocity of the actuator, default value=0
# outputs:
#           u_str - streamtube induction velocity (changed in function)
#           u_act - induction velocity at actuator (changed in function)



# define length scales for actuator/near wake scale
# and streamtube/far wake scale
len_act = 1.*R
len_str = 5.*R


if dynamic:
    # update the reference unperturbed wind speed taking into account
    # the motion of the actuator
    expf=np.exp(-dt*Uref/len_str)
    Uref = Uref*expf+(Uinf-v_actuator)*(1-expf)
else:
    # define the reference velocity as the same as the unperturbed wind speed
    Uref = Uinf

#calculate reference streamtube velocity
Ustr=Uref-(u_act+u_str)/2

# calculate value of forcing function for a
Uqs=np.array(CT/4*Uinf**2/Ustr)

# apply adapted Glauert correction if required
Induction_Glauert=   1-np.sqrt(1.816)/2;

if glauert:
```

https://doi.org/10.5194/wes-2021-34
Preprint. Discussion started: 28 April 2021
© Author(s) 2021. CC BY 4.0 License.

```
        IndGlauert= np.logical_and(Ustr<(Uref*(1-Induction_Glauert )),Uqs>0)
        # IndGlauert -> index of cases that the reference streamtube velocity
        # is lower than the criteria by Glauert and Uqs positive
        Uqs[IndGlauert]=-1.88254912-1.54029217*Uqs[IndGlauert]**(1/2) +\
        4.08622347*Uqs[IndGlauert]**(1/4) # from curve fit of Glauert's
                                          # correction for heavy loaded flow


    # define time scales of convection of the wake for actuator/near wake scale
    # and streamtube/far wake scale. We define them as the inverse of the time
    # scale, to avoid divide by zero due to the velocity of the actuator

    # time of relative convection of old near actuator solution
    inv_tau_act_1 = (Uinf-0.5*u_act-v_actuator)/len_act
    # time of convection of the new generated wake in relation to the actuator
    inv_tau_act_2 = (Uref-0.5*u_act)/len_act
    # time of convection of the old and new wake at stramtube/far wake scale
    inv_tau_str = (Uref-0.5*u_str)/len_str

    # calculate new values of the induction velocity at actuator
    # and streamtube induction velocity
    u_act = u_act*np.exp(-dt*inv_tau_act_1)+Uqs*(1-np.exp(-dt*inv_tau_act_2))
    u_str = u_str*np.exp(-dt*inv_tau_str)+Uqs*(1-np.exp(-dt*inv_tau_str))

    return u_act,u_str,Uref
```

Author contributions. CF imagined, proposed, and developed the ideas, reviewed previous work, proposed the hypothesis and methods, derived and programmed all models, created the simulations, the results and conclusions, and wrote the majority of the text. WY is an expert in dynamic inflow models who provided models for verification and checked consistency of the concept, discussed the idea, and reviewed previous work. AS provided key elements of the literature review, in particular the review of case studies by other authors. AV is a leader on FOWTs, discussed the ideas, and reviewed previous work. All authors contributed to the review process, both scientific and editorial.

Competing interests. No competing interests are present.

https://doi.org/10.5194/wes-2021-34
Preprint. Discussion started: 28 April 2021
© Author(s) 2021. CC BY 4.0 License.

Acknowledgements. CF would like to acknowledge Jing Dong from Delft University of Technology for the stimulating debate who sparked his interest in this topic. Her research was a key trigger for the development of this work.

https://doi.org/10.5194/wes-2021-34
Preprint. Discussion started: 28 April 2021
© Author(s) 2021. CC BY 4.0 License.

References

Burton, T., Jenkins, N., Sharpe, D., and Bossanyi, E.: Wind Energy Handbook, John Wiley & Sons, Ltd, Chichester, UK, https://doi.org/10.1002/9781119992714, 2011.

Chen, Z., Wang, X., Guo, Y., and Kang, S.: Numerical Analysis of Unsteady Aerodynamic Performance of Floating Offshore Wind Turbine under Platform Surge and Pitch Motions, Renewable Energy, 163, 1849–1870, https://doi.org/10.1016/j.renene.2020.10.096, 2021.

Cormier, M., Caboni, M., Lutz, T., Boorsma, K., and Krämer, E.: Numerical Analysis of Unsteady Aerodynamics of Floating Offshore Wind Turbines, Journal of Physics: Conference Series, 1037, 072 048, https://doi.org/10.1088/1742-6596/1037/7/072048, 2018.

De Tavernier, D. and Ferreira, C. S.: A New Dynamic Inflow Model for Vertical-axis Wind Turbines, Wind Energy, 23, 1196–1209, https://doi.org/10.1002/we.2480, 2020.

de Vaal, J., Hansen, M. L., and Moan, T.: Effect of Wind Turbine Surge Motion on Rotor Thrust and Induced Velocity, Wind Energy, 17, 105–121, https://doi.org/10.1002/we.1562, 2014.

Dong, J. and Viré, A.: Comparative Analysis of Different Criteria for the Prediction of Vortex Ring State of Floating Offshore Wind Turbines, Renewable Energy, 163, 882–909, https://doi.org/10.1016/j.renene.2020.08.027, 2021.

Dong, J., Viré, A., Ferreira, C. S., Li, Z., and van Bussel, G.: A Modified Free Wake Vortex Ring Method for Horizontal-Axis Wind Turbines, Energies, 12, 3900, https://doi.org/10.3390/en12203900, 2019.

Farrugia, R., Sant, T., and Micallef, D.: A Study on the Aerodynamics of a Floating Wind Turbine Rotor, Renewable Energy, 86, 770–784, https://doi.org/10.1016/j.renene.2015.08.063, 2016.

Glauert, H.: Airplane Propellers, pp. 169–360, Springer Berlin Heidelberg, Berlin, Heidelberg, https://doi.org/10.1007/978-3-642-91487-4_3, 1935.

Kyle, R., Lee, Y. C., and Früh, W.-G.: Propeller and Vortex Ring State for Floating Offshore Wind Turbines during Surge, Renewable Energy, 155, 645–657, https://doi.org/10.1016/j.renene.2020.03.105, 2020.

Larsen, T. J. and Madsen, H. A.: On the Way to Reliable Aeroelastic Load Simulation on VAWT's, Proceedings of EWEA, 2013, 9, 2013.

Lee, H. and Lee, D.-J.: Effects of Platform Motions on Aerodynamic Performance and Unsteady Wake Evolution of a Floating Offshore Wind Turbine, Renewable Energy, 143, 9–23, https://doi.org/10.1016/j.renene.2019.04.134, 2019.

Madsen, H. A., Larsen, T. J., Pirrung, G. R., Li, A., and Zahle, F.: Implementation of the Blade Element Momentum Model on a Polar Grid and Its Aeroelastic Load Impact, Wind Energy Science, 5, 1–27, https://doi.org/10.5194/wes-5-1-2020, 2020.

Mancini, S., Boorsma, K., Caboni, M., Cormier, M., Lutz, T., Schito, P., and Zasso, A.: Characterization of the Unsteady Aerodynamic Response of a Floating Offshore Wind Turbine to Surge Motion, Wind Energy Science, 5, 1713–1730, https://doi.org/10.5194/wes-5-1713-2020, 2020.

Micallef, D. and Sant, T.: Loading Effects on Floating Offshore Horizontal Axis Wind Turbines in Surge Motion, Renewable Energy, 83, 737–748, https://doi.org/10.1016/j.renene.2015.05.016, 2015.

Pirrung, G. R. and Madsen, H. A.: Dynamic Inflow Effects in Measurements and High-Fidelity Computations, Wind Energy Science, 3, 545–551, https://doi.org/10.5194/wes-3-545-2018, 2018.

Sebastian, T. and Lackner, M.: Analysis of the Induction and Wake Evolution of an Offshore Floating Wind Turbine, Energies, 5, 968–1000, https://doi.org/10.3390/en5040968, 2012.

Sebastian, T. and Lackner, M.: Characterization of the Unsteady Aerodynamics of Offshore Floating Wind Turbines, Wind Energy, 16, 339–352, https://doi.org/10.1002/we.545, 2013.

https://doi.org/10.5194/wes-2021-34
Preprint. Discussion started: 28 April 2021
© Author(s) 2021. CC BY 4.0 License.

Shen, X., Chen, J., Hu, P., Zhu, X., and Du, Z.: Study of the Unsteady Aerodynamics of Floating Wind Turbines, Energy, 145, 793–809, https://doi.org/10.1016/j.energy.2017.12.100, 2018.

Sivalingam, K., Martin, S., and Singapore Wala, A.: Numerical Validation of Floating Offshore Wind Turbine Scaled Rotors for Surge Motion, Energies, 11, 2578, https://doi.org/10.3390/en11102578, 2018.

Sørensen, J. N. and Myken, A.: Unsteady Actuator Disc Model for Horizontal Axis Wind Turbines, Journal of Wind Engineering and Industrial Aerodynamics, 39, 139–149, 1992.

Sørensen, J. N., Shen, W. Z., and Munduate, X.: Analysis of Wake States by a Full-field Actuator Disc Model, Wind Energy: An International Journal for Progress and Applications in Wind Power Conversion Technology, 1, 73–88, 1998.

Tran, T. T. and Kim, D.-H.: A CFD Study into the Influence of Unsteady Aerodynamic Interference on Wind Turbine Surge Motion, Renewable Energy, 90, 204–228, https://doi.org/10.1016/j.renene.2015.12.013, 2016.

van Kuik, G. A. M.: The Fluid Dynamic Basis for Actuator Disc and Rotor Theories, https://doi.org/10.3233/978-1-61499-866-2-i, 2018.

van Kuik, G. A. M.: On the Velocity at Wind Turbine and Propeller Actuator Discs, Wind Energy Science, 5, 855–865, https://doi.org/10.5194/wes-5-855-2020, 2020.

Wen, B., Tian, X., Dong, X., Peng, Z., and Zhang, W.: Influences of Surge Motion on the Power and Thrust Characteristics of an Offshore Floating Wind Turbine, Energy, 141, 2054–2068, https://doi.org/10.1016/j.energy.2017.11.090, 2017.

Yu, W.: The Wake of an Unsteady Actuator Disc, Ph.D. thesis, Delft University of Technology, https://doi.org/10.4233/UUID:0E3A2402-585C-41B1-81CF-A35753076DFC, 2018.

Yu, W., Ferreira, C., van Kuik, G., and Baldacchino, D.: Verifying the Blade Element Momentum Method in unsteady, radially varied, axisymmetric loading using a vortex ring model, Wind Energy, 20, 269–288, https://doi.org/10.1002/we.2005, 2016.